



Deletion of H-ferritin in macrophages alleviates obesity and diabetes induced by high-fat diet in mice

Yasumasa Ikeda¹ · Hiroaki Watanabe^{1,2} · Tetsuya Shiuchi³ · Hirofumi Hamano⁴ · Yuya Horinouchi¹ · Masaki Imanishi⁴ · Mitsuhiro Goda⁴ · Yoshito Zamami^{2,4} · Kenshi Takechi⁵ · Yuki Izawa-Ishizawa⁶ · Licht Miyamoto⁷ · Keisuke Ishizawa^{2,4} · Ken-ichi Aihara⁸ · Koichiro Tsuchiya⁷ · Toshiaki Tamaki^{1,9}

Received: 14 October 2019 / Accepted: 9 March 2020 / Published online: 19 May 2020

© Springer-Verlag GmbH Germany, part of Springer Nature 2020

Abstract

Aims/hypothesis Iron accumulation affects obesity and diabetes, both of which are ameliorated by iron reduction. Ferritin, an iron-storage protein, plays a crucial role in iron metabolism. H-ferritin exerts its cytoprotective action by reducing toxicity via its ferroxidase activity. We investigated the role of macrophage H-ferritin in obesity and diabetes.

Methods Conditional macrophage-specific H-ferritin (*Fth*, also known as *Fth1*) knockout (LysM-Cre *Fth* KO) mice were used and divided into four groups: wild-type (WT) and LysM-Cre *Fth* KO mice with normal diet (ND), and WT and LysM-Cre *Fth* KO mice with high-fat diet (HFD). These mice were analysed for characteristics of obesity and diabetes, tissue iron content, inflammation, oxidative stress, insulin sensitivity and metabolic measurements. RAW264.7 macrophage cells were used for in vitro experiments.

Results Iron concentration reduced, and mRNA expression of ferroportin increased, in macrophages from LysM-Cre *Fth* KO mice. HFD-induced obesity was lower in LysM-Cre *Fth* KO mice than in WT mice at 12 weeks (body weight: KO 34.6 ± 5.6 g vs WT 40.1 ± 5.2 g). mRNA expression of inflammatory cytokines and infiltrated macrophages and oxidative stress increased in the adipose tissue of HFD-fed WT mice, but was not elevated in HFD-fed LysM-Cre *Fth* KO mice. However, WT mice fed an HFD had elevated iron concentration in adipose tissue and spleen, which was not observed in LysM-Cre *Fth* KO mice fed an HFD (adipose tissue [$\mu\text{mol Fe/g protein}$]: KO 1496 ± 479 vs WT 2316 ± 866 ; spleen [$\mu\text{mol Fe/g protein}$]: KO 218 ± 54 vs WT 334 ± 83). Moreover, HFD administration impaired both glucose tolerance and insulin sensitivity in WT mice, which was ameliorated in LysM-Cre *Fth* KO mice. In addition, energy expenditure, mRNA expression of thermogenic genes, and body temperature were higher in KO mice with HFD than WT mice with HFD. In vitro experiments showed that iron content was reduced, and lipopolysaccharide-induced *Tnf- α* (also known as *Tnf*) mRNA upregulation was inhibited in a macrophage cell line transfected with *Fth* siRNA.

Conclusions/interpretation Deletion of macrophage H-ferritin suppresses the inflammatory response by reducing intracellular iron levels, resulting in the prevention of HFD-induced obesity and diabetes. The findings from this study highlight macrophage iron levels as a potential therapeutic target for obesity and diabetes.

Keywords Diabetes · H-ferritin · Inflammation · Iron · Macrophage · Obesity

Yasumasa Ikeda and Hiroaki Watanabe contributed equally to this work.

✉ Yasumasa Ikeda
yasuike@tokushima-u.ac.jp

¹ Department of Pharmacology, Institute of Biomedical Sciences, Tokushima University Graduate School, 3-18-15 Kuramoto-cho, Tokushima 770-8503, Japan

² Department of Clinical Pharmacology, Institute of Biomedical Sciences, Tokushima University Graduate School, Tokushima, Japan

³ Department of Integrative Physiology, Institute of Biomedical Sciences, Tokushima University Graduate School, Tokushima, Japan

⁴ Department of Pharmacy, Tokushima University Hospital, Tokushima, Japan

⁵ Clinical Trial Center for Developmental Therapeutics, Tokushima University Hospital, Tokushima, Japan

⁶ AWA Support Center, Tokushima University, Tokushima, Japan

⁷ Department of Medical Pharmacology, Institute of Biomedical Sciences, Tokushima University Graduate School, Tokushima, Japan

⁸ Department of Community Medicine for Diabetes and Metabolic Disorders, Institute of Biomedical Sciences, Tokushima University Graduate School, Tokushima, Japan

⁹ Anan Medical Center, Tokushima, Japan

Research in context

What is already known about this subject?

- Increased body iron content is related to obesity and diabetes, both of which are ameliorated by iron reduction. However, iron-deficient anaemia is induced by non-specific iron reduction
- Macrophages play a key role in the pathogenesis of obesity and diabetes through chronic inflammation
- The proinflammatory M1 macrophage phenotype involves intracellular iron retention, with the divergent expression of iron-related proteins and iron content in macrophages

What is the key question?

- Does the reduction of macrophage iron content ameliorate obesity and diabetes by reducing the inflammatory response?

What are the new findings?

- Conditional gene deletion of H-ferritin results in the reduction of iron content in macrophages and spleen without concomitant anaemia
- High-fat diet-induced obesity and diabetes were less frequent in macrophage-specific H-ferritin knockout mice
- The knockout mice showed fewer inflammatory changes and less oxidative stress in adipose tissue

How might this impact on clinical practice in the foreseeable future?

- Control of iron levels in macrophages is a potential therapeutic target for obesity and diabetes

Abbreviations

ERK1/2	Extracellular signal-regulated kinase 1/2
FPN	Ferroportin
FTH	Ferritin heavy chain (H-ferritin)
FTL	Ferritin light chain (L-ferritin)
HFD	High-fat diet
HNE	Hydroxynonenal
IR β	Insulin receptor β
JNK	c-Jun N-terminal kinase
KO	Knockout
LPS	Lipopolysaccharide
LysM	Lysozyme M
MAPK	Mitogen-activated protein kinase
ND	Normal diet
SAPK	Stress-activated protein kinase
siRNA	Small interfering RNA
TfR	Transferrin receptor
WT	Wild-type

Introduction

Iron is an essential micromineral for all living beings. However, an excessive amount of iron induces oxidative stress by catalysing toxic hydroxy-radical production via the Fenton reaction. In hereditary iron overload disorders, cardiomyopathy, hepatic injury and diabetes are caused by oxidative stress via ectopic tissue accumulation of excess iron [1].

Increased body iron content can be related to many diseases, including liver disease [2, 3], obesity [4], diabetes [5], cardiovascular disease [6, 7] and kidney disease [8]. Therefore, iron reduction could be an effective strategy for ameliorating the pathological conditions in such diseases, as shown by both clinical [9, 10] and experimental studies [11–14]. Whole body iron reduction causes iron-deficient anaemia; therefore, more specific iron reduction is an important strategy to avoid iron deficiency.

In terms of the dynamics of iron metabolism, iron is mostly recycled in the human body, since daily iron intake and excretion are only 1–1.5 mg each. Body iron is mostly located in erythrocytes (>70%) as haemoglobin. Macrophages phagocytise senescent erythrocytes and release iron obtained from haemoglobin into circulation, where it binds to plasma transferrin [15]. Thus, macrophages are central regulators of body iron homeostasis through the recycling of iron.

Macrophages undergo polarisation to form either the proinflammatory phenotype (M1: classically activated) or the anti-inflammatory phenotype (M2: alternatively activated) [16]. These two phenotypes are characterised by divergent expression of iron-related proteins and iron content [17, 18]. M1 macrophages have increased iron content through the expression of high levels of the iron-storage protein, H-ferritin (ferritin heavy chain; FTH) and low levels of the iron export protein ferroportin (FPN). In contrast, M2 macrophages have low iron content expression with low levels of H-ferritin and high levels of FPN. Differences in polarisation between M1 and

M2 macrophages may involve intracellular iron content, affecting macrophage function, especially in the aspect of proinflammatory change [19]. We found that FTH protein expression colocalises with the increase in infiltrated macrophages in the adipose tissue of obese KKAY mice [11]. Additionally, increased iron content enhances the lipopolysaccharide (LPS)-induced inflammatory cytokine production in hepatic macrophages [20], and an iron chelator (deferrioxamine) suppresses cytokine production in mouse bone marrow macrophages [21]. We hypothesised that the coordination of ferritin and intracellular iron is a determining factor in the polarisation of macrophages to the inflammatory phenotype.

In this study, we aimed to explore the role of macrophage FTH in obesity and diabetes induced by high-fat diet using macrophage-specific *Fth* (also known as *Fth1*) knockout mice.

Methods

Animal preparation and procedures Floxed *Fth* mice (B6.129-*Fth1*^{tm1.1Lck}) (C57BL/6J background) were purchased from Jackson Laboratory (Bar Harbor, ME, USA). Lysozyme M (LysM)-Cre mice (B6.129P2-*Ly2*^{tm1(cre)Jfo}) (C57BL/6J background) were provided by K-i Aihara (Tokushima University). This cross-generated mouse carries both the *cre* gene and the heterozygous floxed *Fth* gene (LysM-Cre *Fth*^{fl/+}). These mice were further mated with floxed *Fth* mice to generate LysM-Cre *Fth* knockout (KO) mice. Floxed *Fth* littermate mice without the LysM-Cre gene were used as control wild-type (WT) mice. The male mice were randomly divided into the following four groups at 6 weeks of age: WT mice fed with control (normal) diet (ND; AIN-93 M, Oriental Yeast Co., Tokyo, Japan); LysM-Cre *Fth* KO mice fed with ND; WT mice fed with high-fat diet (HFD; HFD-60, Oriental Yeast Co.); and LysM-Cre *Fth* KO mice fed with HFD. The mice were maintained with ad libitum access to water and the corresponding diet. Twelve weeks later, the mice were euthanised by intraperitoneally injecting an overdose of anaesthesia, and tissues were removed and stored at -80°C until further use. All experimental procedures for mice were performed in accordance with the guidelines of the Animal Research Committee of Tokushima University Graduate School, and the protocol was approved by the Institutional Review Board of Tokushima University Graduate School for animal protection (Permit Number: T28–49).

Peritoneal macrophage isolation After anaesthesia, mice were intraperitoneally injected with 10 ml sterilised PBS. The abdomen was gently massaged for 5 min, and then PBS was recovered. Collected intraperitoneal PBS was centrifuged at 1.4 g, incubated with erythrocyte lysis buffer for 5 min, and washed and re-centrifuged with fresh PBS twice.

Extraction of tissues after insulin stimulation After a 24 h fasting, mice under anaesthesia were injected with 1 U/kg insulin through the inferior vena cava. After 3 min, epididymal fat, liver and gastrocnemius muscle were immediately removed and used for analysis.

Cell culture and small interfering RNA transfection RAW264.7 mouse macrophage cells were purchased from DS Pharma Biomedical Co. (Osaka, Japan), and were maintained and sub-cultured in DMEM containing 10% FBS, according to the culture protocol. Small interfering RNA (siRNA) targeting mouse *Fth* and a non-targeting siRNA control sequence were purchased from Dharmacon (Horizon Discovery, Cambridge, UK). Transfection of siRNA was performed as described previously [22]. Cells were used for further experiments after 48 h of transfection and then stimulated with 100 ng/ml LPS (FUJIFILM Wako Pure Chemical Corporation, Osaka, Japan) for 2 h. The cells were confirmed not to be contaminated with mycoplasma.

RNA extraction and mRNA expression analysis The methods used for RNA extraction, cDNA synthesis, and quantitative RT-PCR have been previously described [11]. Briefly, the tissues or cells were homogenised in RNaiso reagent (Takara Bio, Otsu, Japan). RNA extraction and cDNA synthesis were performed according to the manufacturer's instructions (PrimeScript RT reagent kit with gDNA Eraser [Perfect Real Time], Takara Bio). Quantitative RT-PCR was performed using the CFX Connect Real-Time PCR Detection System (Bio-Rad Laboratories, Hercules, CA, USA) with SYBR Green (THUNDERBIRD SYBR qPCR Mix, TOYOBO Co., Osaka, Japan). The mRNA expression levels were normalised using *36B4* (also known as *Rplp0*) expression, and the values were compared with the control group in terms of relative fold change. The primer sets used are shown in Table 1.

Protein extraction and western blot analysis Protein preparation and western blotting were performed as previously described in detail [11]. Tissue or cell samples were homogenised or sonicated in a protein lysis buffer containing proteinase inhibitors and a phosphatase inhibitor. The extracted proteins were boiled for 5 min in Laemmli sample buffer and used for western blotting. The visualised immunoreactive protein bands were semi-quantified by densitometric analysis using Image J software (version 1.38, NIH, Bethesda, MD, USA). We used Can Get Signal Solution 1 (TOYOBO Co.) as dilution buffer for primary antibodies, and 0.5% skimmed milk in PBS-T as dilution buffer for secondary antibodies. The following commercially available antibodies were used: anti-FTH, anti-ferritin light chain (FTL), anti-p22^{phox} (Santa Cruz Biotechnology, Dallas, TX, USA), anti-phospho-stress-

Table 1 Primer sequences

	Forward	Reverse
<i>Fth</i>	TGATGAAGCTGCAGAACCAG	GTGCACACTCCATTGCATTC
<i>Ftl</i>	AATGGGGTAAAACCCAGGAG	AGATCCAAGAGGGCCTGATT
<i>Hmox1</i>	TGCTCGAATGAACACTCTGG	AAGGCGGTCTTAGCCTC
<i>Fpn</i>	CCCTGCTCTGGCTGTAAG	GGTGGGCTCTTGTTCACATT
<i>Tfr</i>	CCGAGAGGAGACTTCACAG	TCCACGATTTCCAGAGAAC
<i>Tnf-α</i>	ACGGCATGGATCTCAAAGAC	GTGGGTGAGGAGCACGTAGT
<i>Mcp-1</i>	GGAGCTCATGATGTGAGCAA	GACCAGGCAAGGGAATTACA
<i>Il-1β</i>	CAGGCAGGCAGTATCACTCA	TGTCCTCATCTGGAAGGTC
<i>Il-6</i>	CCGGAGAGGAGACTTCACAG	TCCACGATTTCCAGAGAAC
<i>F4/80</i>	CTGTAACCGGATGGCAAAC	CTGTACCCACATGGCTGATG
<i>Cd11c</i>	ATTTCTGAGAGCCAGACGA	CCATTTGCTTCTCCAACAT
<i>Cd68</i>	CTTCCCACAGGCAGCACAG	AATGATGAGAGGCAGCAAGAGG
Adiponectin	GTTGCAAGCTCTCTGTTC	ATCCAACCTGCACAAGTTC
Leptin	TGACACAAAACCTCATCA	TGAAGCCCAGGAATGAAGTC
<i>Cyba</i>	GTGGACTCCCA TTGAGCCTA	CTCCTCTTACCCTCACTCG
<i>Ucp1</i>	TCTCAGCCGGCTTAATGACT	TGCATTCTGACCTTCACGAC
<i>Ucp3</i>	AGCCCTCTGCACTGTATGCT	AAAGGAGGGCACAATCCTT
<i>Adrb3</i>	ACAGGAATGCCACTCCAATC	AAGGAGACGGAGGAGGAGAG
<i>Ppargc1a</i>	CCGAGAATTCATGGAGCAAT	TTTCTGTGGGTTTGGTGTGA
<i>Dio2</i>	GATGCTCCCAATCCAGTGT	TGAACCAAAGTTGACCACCA
<i>Prdm16</i>	TGGGCTCACTACCCTACCAC	GACTTTGGCTCAGCCTTGAC
<i>Cidea</i>	CTCGGCTGTCTCAATGTCAA	GGAAGTGTCCCCTCATCTGT
<i>36B4</i>	GCTCCAAGCAGATGCAGCA	CCGGATGTGAGGCAGCAG

activated protein kinase (SAPK)/c-Jun N-terminal kinase (JNK) (Thr183/Tyr185), anti-total SAPK/JNK, anti-phospho-p44/42 mitogen-activated protein kinase (extracellular signal-regulated kinase 1/2 [ERK1/2]), anti-total p44/42 MAPK (ERK1/2), anti-phospho-Akt, anti-total Akt, anti-phospho-insulin receptor β (IR β), anti-total IR β (Cell Signaling Technology, Danvers, MA, USA), and anti- α -tubulin (protein loading control; Merck, Darmstadt, Germany). Anti-rabbit IgG, HRP-linked Antibody (Cell Signaling Technology [7074]), goat anti-mouse IgG-HRP-linked antibody (Santa Cruz Biotechnology [sc-2005]), and donkey anti-goat IgG-HRP-linked antibody (Santa Cruz Biotechnology [sc-2020]) were used for secondary antibodies. Details of dilutions used for antibodies are available in Table 2.

Histological analysis of adipocyte size Epididymal fat tissue was fixed in 4% paraformaldehyde. After defatting and paraffin-embedding, the samples were cut into 3 μ m thick sections and stained with haematoxylin–eosin. Adipocyte size was determined by ten random fields in the sections for each mouse [11].

Haematological analysis and blood chemistry Whole blood cell counts were performed by Shikoku Chuken (Kagawa,

Japan). Blood glucose and insulin levels were measured by using an ACCU-CHEK Aviva Kit (Roche Diagnostics, Basel, Switzerland) and a Mouse Insulin ELISA Kit (Morinaga Institute of Biological Science, Yokohama, Japan), respectively [11]. Plasma levels of TNF- α and adiponectin were determined using commercial ELISA kits (Quantikine ELISA Kit, R&D Systems, Minneapolis, MN, USA).

Glucose tolerance test After fasting for 24 h, mice were intraperitoneally injected with 20% glucose solution (2.0 g/kg body weight). Blood was obtained from a tail vein at scheduled time points (0, 30, 60 and 120 min), and blood glucose levels were measured [11].

Insulin tolerance test After a 4 h fast, the mice were subjected to an insulin tolerance test. They were injected intraperitoneally with insulin (0.75 U/kg body weight; Humulin R; Eli Lilly, Indianapolis, IN, USA). Blood glucose levels were measured at scheduled times (0, 15, 30, 60 and 120 min) [11].

Immunohistochemistry of macrophages in adipose tissues Immunohistochemical staining of F4/80 (MCA497GA, Bio-Rad Laboratories, Tokyo, Japan) was performed as described previously [11]. To evaluate macrophage infiltration, ten

Table 2 Primary antibodies used for Western blots

Protein	Supplier and catalogue no.	First dilution	Second dilution
FTH	Santa Cruz (sc-14416)	1:250	1:50,000
FTL	Santa Cruz (sc-14422)	1:250	1:50,000
p22 ^{phox}	Santa Cruz (sc-20781)	1:250	1:50,000
Phospho-JNK	CST (9251)	1:500	1:50,000
Total-JNK	CST (9252)	1:1000	1:50,000
Phospho-ERK1/2	CST (9101)	1:1000	1:50,000
Total-ERK1/2	CST (9102)	1:1000	1:50,000
Phospho-Akt	CST (9271)	1:500	1:50,000
Total-Akt	CST (9272)	1:1000	1:50,000
Phospho- IR β	CST (3024)	1:1000	1:25,000
Total- IR β	CST (3025)	1:1000	1:25,000
α -Tubulin	Merck (CP06)	1:1000	1:100,000

microscopic fields were randomly selected and F4/80-positive cells were counted.

Detection of oxidative stress in adipose tissue Oxidative stress was evaluated by anti-4-hydroxynonenal (HNE) staining (MHN-100P, Japan Institute for the Control of Aging (JaICA), Nikken SEIL Co., Shizuoka, Japan). In brief, paraffin sections were deparaffinised and rehydrated, and then boiled with antigen retrieval 10 mmol/l citrate buffer for 10 min and cooled for 20 min. After blocking, sections were incubated with 4-HNE antibody (1:50) at 4°C overnight. Antibody distribution was visualised using immunofluorescence (Alexafluor; Life Technologies, Tokyo, Japan). Sections incubated without primary antibody were used as negative controls.

Measurement of iron content Tissue iron content was measured using an iron assay kit (Metallo assay, Metallogenics, Chiba, Japan) [12]. Iron concentration was corrected using protein concentration and expressed as $\mu\text{mol Fe per g protein concentration}$.

Metabolic measurement and body temperature ARCO-2000 (ARCO System, Chiba, Japan) was used to measure $\dot{V}O_2$ and RQ. Mice were placed in ACTIMO-100 N (SHINFACTORY Co., Fukuoka, Japan) with free access to food and water, allowing them to acclimatise in individual metabolic cages for 72 h before any measurements. The data were acquired at 12 h intervals for 24 h. A rectal probe (BP98A Softron Corp., Tokyo, Japan) measured the body temperature of mice.

Statistical analysis In vivo studies were carried out with at least three independent experiments in each group and sample replication of in vivo data was obtained from individual mice. In vitro studies were done at least twice in independent experiments. Blinding to group assignment and outcome

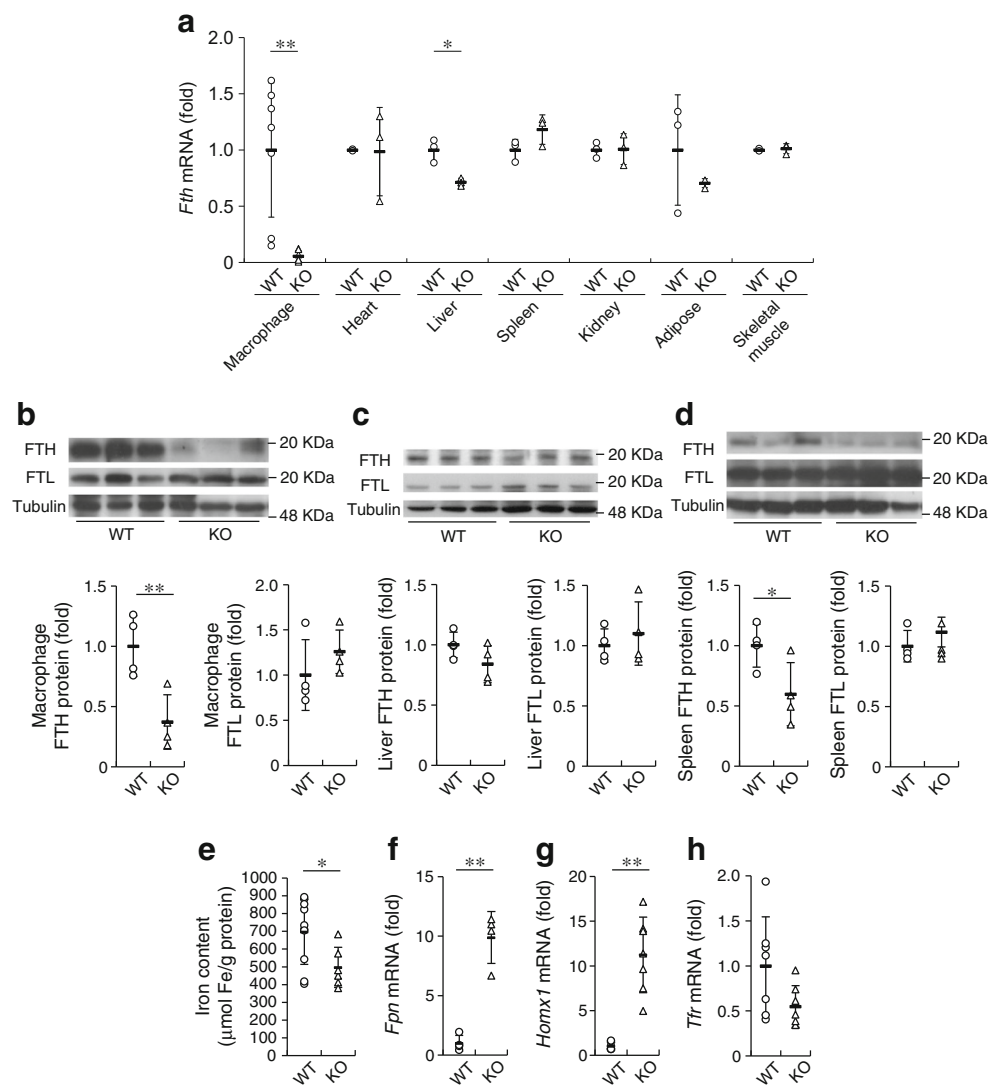
assessment were not carried out in these studies. There were no criteria for exclusion of any data, and no results were intentionally removed. Data are presented as mean \pm SD. An unpaired, two-tailed, Student's *t* test was used for comparison between the two groups. For comparison between more than two groups, the statistical significance of each difference was evaluated using a post hoc test (either Dunnett's method or Tukey–Kramer's method). Statistical significance was set at $p < 0.05$.

Results

Characteristics of LysM-Cre *Fth* KO mice and WT mice First, we examined the *Fth* deletion in macrophages and other tissues. As shown in Fig. 1a, *Fth* mRNA was deleted in peritoneal macrophages and was reduced by around 25% in liver samples. There was no difference detected in *Fth* mRNA expression in the heart, spleen, kidney, adipose tissue and skeletal muscles between WT and LysM-Cre *Fth* KO mice. In terms of ferritin protein, FTH protein expression was reduced in macrophages and spleen, but not in the liver of KO mice, and there was no difference in FTL protein expression in macrophages, liver or spleen between WT and KO mice (Fig. 1b–d).

Iron concentration and iron-related gene expression in macrophages In peritoneal macrophages, the iron concentration was lower in LysM-Cre *Fth* KO mice than in WT mice (Fig. 1e). *Fpn* (also known as *Slc40a1*) and *Homx1* mRNA expression increased, whereas *Tfr* (also known as *Tfrc*) mRNA expression showed a decrease in macrophages in KO mice (Fig. 1f–h). These results suggest that the *Fth* gene deletion leads to reduced intracellular iron concentration through a decrease in iron import and an increase in iron export in macrophages.

Fig. 1 The differences of ferritin expression in various tissues between WT mice and LysM-Cre *Fth* KO mice. **(a)** *Fth* mRNA expression in macrophage, heart, liver, spleen, kidney, adipose tissue and skeletal muscle. Values are expressed as mean \pm SD; * p < 0.05, ** p < 0.01; n = 3–7 in each group. **(b–d)** FTH and FTL protein expression in macrophages **(b)**, liver **(c)** and spleen **(d)**. Values are expressed as mean \pm SD; * p < 0.05, ** p < 0.01; n = 4 in each group. **(e)** Iron content in macrophages. Values are expressed as mean \pm SD; * p < 0.05; n = 6–10 in each group. **(f–h)** mRNA expression of *Fpn* **(f)**, *Homx1* **(g)** and *Tfr* **(h)** in macrophages. Values are expressed as mean \pm SD; ** p < 0.01; n = 4–7 in each group. There was no significant difference in *Tfr* mRNA between WT and KO (p = 0.08)

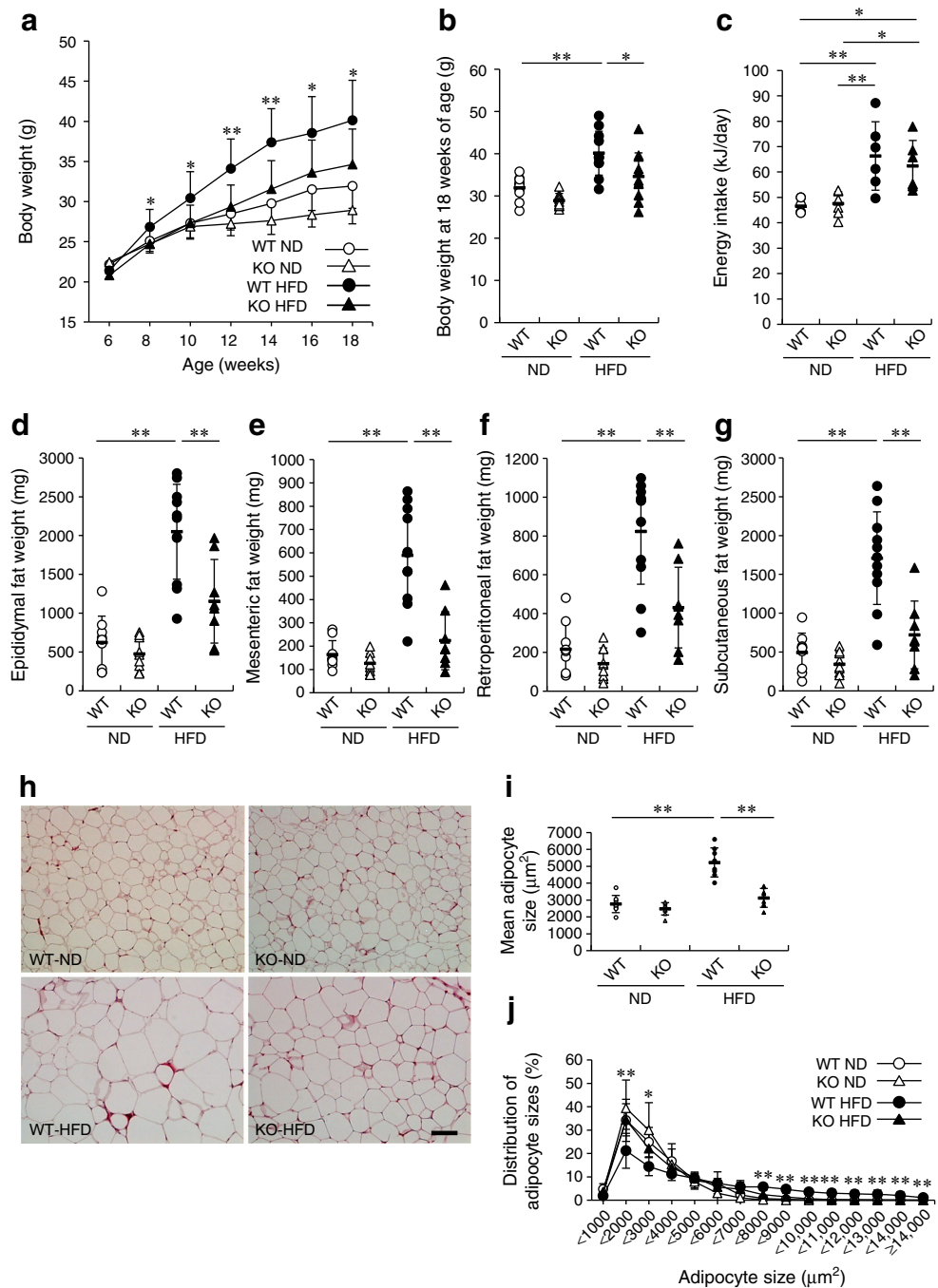


Effect of macrophage *Fth* deletion on body weight and adipose tissues Next, we tested the role of the macrophage *Fth* gene on HFD-induced obesity and diabetes. No difference was seen in body weight gained during the experimental course between WT mice and LysM-Cre *Fth* KO mice. The body weight of WT mice fed an HFD increased after 2 weeks, whereas this increase was suppressed in KO mice at 12 weeks (body weight: KO 34.6 \pm 5.6 g vs WT 40.1 \pm 5.2 g) (Fig. 2a,b). There was no difference in the daily energy intake between WT mice and KO mice in the HFD-fed group (Fig. 2c). The HFD-induced increase in weight of adipose tissue was attenuated in KO mice compared with WT mice (Fig. 2d–g). In histological analysis, HFD feeding resulted in enlarged adipocyte size in epididymal fat, and this increase was smaller in KO mice than in WT mice (Fig. 2h,i). The distribution of adipocyte size indicated that LysM-Cre *Fth* KO mice fed with HFD increased the proportion of small-sized adipocytes and decreased the proportion of large-sized adipocytes

compared with WT mice fed with HFD (Fig. 2j). Additionally, erythrocytes, haemoglobin and haematocrit were elevated in HFD-fed mice, and there was no difference in these variables between WT mice and LysM-Cre *Fth* KO mice regardless of ND or HFD (Table 3).

Macrophage infiltration and inflammatory cytokine expression in adipose tissue As shown in Fig. 3a and b, the number of F4/80-positive cells was increased in epididymal fat of HFD-fed WT mice, and this was significantly inhibited in HFD-fed KO mice. Similar to the results of immunohistochemical analysis, mRNA expression of *F4/80* (also known as *Adgre1*) and *Cd68* was increased in epididymal fat of HFD-fed WT mice, and they were significantly inhibited in HFD-fed KO mice (Fig. 3c,d). The mRNA expression of inflammatory cytokines such as *Tnf- α* (also known as *Tnf*), *Mcp-1* (also known as *Ccl2*), *Il-1 β* (also known as *Il1b*) and *Il-6*, were upregulated in epididymal fat of WT mice with HFD, but were diminished in KO mice with HFD (Fig. 3f–i). Adiponectin

Fig. 2 Body weight, fat weight and adipocyte size and distribution. **(a)** Changes in body weight in WT mice and LysM-Cre *Fth* KO mice fed with ND or HFD. Values are expressed as mean \pm SD. * p <0.05, ** p <0.01 for WT HFD vs LysM-Cre *Fth* KO mice fed HFD; n =9–11 in each group. **(b)** Body weight at 12 weeks on diet (18 weeks of age). Values are expressed as mean \pm SD; * p <0.05, ** p <0.01; n =9–11 in each group. **(c)** Daily energy intake. Values are expressed as mean \pm SD; * p <0.05, ** p <0.01; n =6–7 in each group. **(d–g)** Weight of epididymal fat **(d)**, mesenteric fat **(e)**, retroperitoneal fat **(f)** and subcutaneous fat **(g)** at 12 weeks on diet. Values are expressed as mean \pm SD; ** p <0.01; n =9–11 in each group. **(h)** Representative findings with haematoxylin–eosin staining of adipocytes in epididymal fat; scale bar, 100 μ m. **(i)** Mean adipocyte size. Values are expressed as mean \pm SD; ** p <0.01; n =8 in each group. **(j)** Distribution of adipocyte sizes. Values are expressed as mean \pm SD; * p <0.05, ** p <0.01 for WT HFD vs WT mice fed with ND, LysM-Cre *Fth* KO mice fed with ND and LysM-Cre *Fth* KO mice fed with HFD; n =8 in each group



(*Adipoq*) mRNA expression was reduced, and leptin (*Lep*) mRNA expression was increased in the fat of HFD-fed WT mice, while these changes were ameliorated in HFD-fed KO mice (Fig. 3j,k). Additionally, mRNA expression of *Cd11c* (also known as *Itgax*), a surface marker of M1-like cells, was elevated in HFD-fed WT mice, but this increase was inhibited in HFD-fed KO mice (Fig. 3e). In plasma, the HFD-induced increase in the TNF- α levels and decrease in adiponectin levels were also ameliorated in KO mice (Fig. 3l,m). These results suggested that macrophage *Fth* deletion leads to inhibition of HFD-

induced inflammation and the disorder of adipocytokines in fat.

Effect of macrophage *Fth* deletion on MAPK pathway and oxidative stress JNK and ERK1/2, members of the MAPK family, play an important role in inflammatory gene regulation [23]. Administration of HFD increased the phosphorylated levels of JNK, but not ERK1/2, in the fat of WT mice, and this was suppressed in KO mice (Fig. 4a–c). In adipose tissue, 4-HNE intensity was augmented in WT mice with HFD, and this increase was suppressed in HFD-fed KO mice (Fig. 4d,e).

Table 3 Erythrocyte count, haemoglobin, haematocrit, mean corpuscular volume, mean corpuscular haemoglobin and mean corpuscular haemoglobin concentration in each mouse group

	WT-ND	LysM-Cre <i>Fth</i> KO-ND	WT-HFD	LysM-Cre <i>Fth</i> KO-HFD
Erythrocytes ($\times 10^4/\mu\text{l}$)	783 \pm 53	767 \pm 101	881 \pm 69**‡	901 \pm 115**‡
Haemoglobin (g/l)	115 \pm 8	117 \pm 4	132 \pm 11***‡	134 \pm 17**‡
Haematocrit (l)	0.361 \pm 0.030	0.363 \pm 0.038	0.414 \pm 0.035*‡	0.412 \pm 0.063*‡
MCV (fl)	46.1 \pm 2.2	47.6 \pm 2.5	45.9 \pm 1.6	45.5 \pm 1.8
MCH (pg/cell)	14.7 \pm 0.4	15.2 \pm 0.5*	15.0 \pm 0.6	14.8 \pm 0.4
MCHC (g/l)	318 \pm 9	321 \pm 9	328 \pm 9	326 \pm 13
Blood glucose (mmol/l)	4.2 \pm 0.6	4.3 \pm 0.5	6.1 \pm 1.0***‡	4.7 \pm 0.8††
Plasma insulin (pmol/l)	18.8 \pm 2.1	29.2 \pm 22.2	428.5 \pm 355.6***‡	163.9 \pm 256.3†

Data represent mean \pm SD; $n = 10$ – 15 in each group

* $p < 0.05$, ** $p < 0.01$ vs WT-ND; ‡ $p < 0.05$, ‡‡ $p < 0.01$ vs LysM-Cre *Fth* KO-ND; † $p < 0.05$, †† $p < 0.01$ vs WT-HFD

MCH, mean corpuscular haemoglobin; MCHC, mean corpuscular haemoglobin concentration; MCV, mean corpuscular volume

NADPH oxidase is a source of reactive oxygen species, and increase in p22^{phox} protein, an NADPH oxidase subunit with haem protein, was suppressed by iron reduction in adipose tissue from obese mice [11]. In line with this, p22^{phox} was elevated in adipose tissue of HFD-fed WT mice, and this increase was suppressed in adipose tissue of HFD-fed KO mice (Fig. 4f,g). Thus, HFD-induced inflammatory pathway activation and oxidative stress were inhibited in the fat of KO mice.

Iron content in fat, spleen and macrophages In epididymal fat and spleen, tissue iron content was elevated in HFD-fed WT mice, and this was inhibited in HFD-fed KO mice (adipose tissue [$\mu\text{mol Fe/g protein}$]: KO 1496 \pm 479 vs WT 2316 \pm 866; spleen [$\mu\text{mol Fe/g protein}$]: KO 218 \pm 54 vs WT 334 \pm 83) (Fig. 4h,i). Iron content in macrophages was lower in KO mice than in WT mice. However, macrophage iron levels did not change by HFD in WT and KO mice (Fig. 4j).

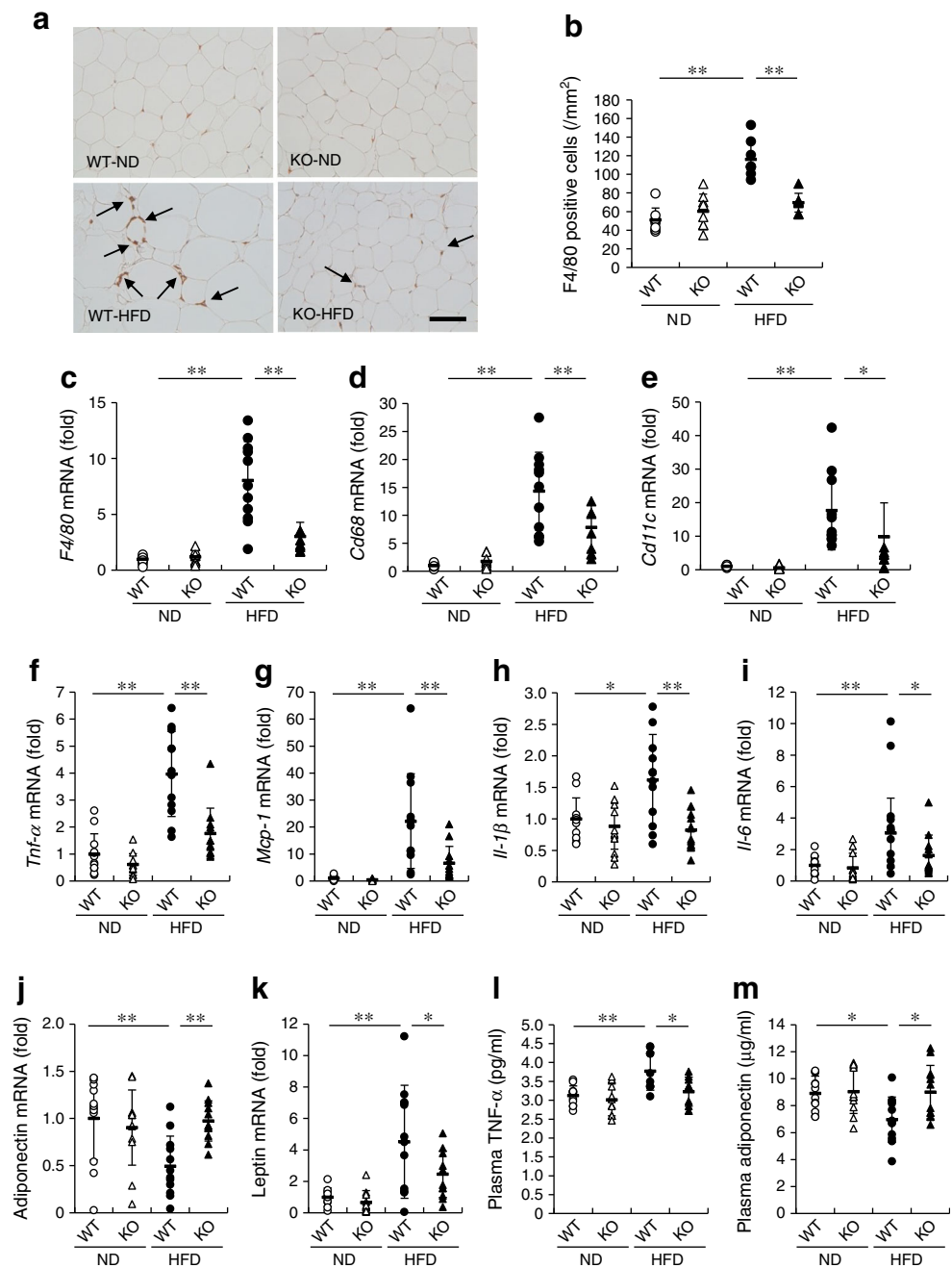
Macrophage *Fth* deletion on glucose tolerance, insulin sensitivity and insulin signalling pathway To examine whether macrophage *Fth* deletion affected glucose tolerance and insulin sensitivity, we subjected mice to IPGTT and IPITT, respectively. There was no difference in blood glucose levels between WT mice and KO mice in ND-fed groups after glucose injection, and the degree of increase in blood glucose level after glucose injection was lower in HFD-fed KO mice than in HFD-fed WT mice (Fig. 5a,b). With IPITT, the reduction in blood glucose levels was more in KO mice than in WT mice in HFD-fed groups, and there was no difference in blood glucose levels between WT mice and KO mice in ND-fed groups after insulin injection (Fig. 5c,d). The phosphorylation of the IR β –Akt signalling pathway was increased in epididymal fat in ND-fed groups of both WT mice and KO mice after insulin stimulation. Phosphorylated levels of IR β –Akt signalling after insulin stimulation was diminished in HFD-fed WT

mice, and it was ameliorated in the fat of HFD-fed KO mice (Fig. 5e,f). Similarly to fat, the reduced phosphorylation of IR β –Akt signalling after insulin stimulation was also ameliorated in the liver and skeletal muscle of HFD-fed KO mice (Fig. 6a–f). The mRNA expression of inflammatory cytokines (except for *Il-6*) was increased in liver and skeletal muscle of HFD-fed WT mice, but this was not seen in those tissues of HFD-fed KO mice (Fig. 6g–n). The fasting plasma glucose level was significantly higher in HFD-fed WT mice than in HFD-fed KO mice. The plasma insulin level was markedly elevated in HFD-fed WT mice; in HFD-fed KO mice, the levels were significantly lower than in HFD-fed KO mice (Table 3). These results suggest that macrophage *Fth* deletion leads to the improvement in glucose tolerance and insulin resistance both through inhibiting inflammation and maintaining insulin signalling in fat, liver and skeletal muscle in obesity and diabetes.

Effect of macrophage *Fth* deletion on energy expenditure in mice fed with HFD We further analysed energy expenditure. $\dot{V}O_2$ and energy expenditure were significantly higher in HFD-fed KO mice during the dark phase, while RQ was lower in HFD-fed KO mice compared with HFD-fed WT mice during the dark and total phase (Fig. 7a–c). Additionally, body temperature, as well as the expression of several thermogenic genes (*Ucp3*, *Adrb3*, *Ppargc1a*, *Dio2*, and *Prdm16*) in fat, was significantly higher in HFD-fed KO mice compared with HFD-fed WT mice (Fig. 7d–k). These results partly contributed to the decreased body-weight gain in HFD-fed KO mice.

Effect of *Fth* deletion on LPS-induced inflammation in vitro experiments We examined the effect of *Fth* deletion by using RAW264.7 cells derived from mouse peritoneal macrophages. siRNA targeting *Fth* gene transduction reduced *Fth* mRNA by approximately 20% and mimicked the phenotype of iron-related genes and iron content in macrophages of

Fig. 3 Effect of macrophage *Fth* deletion on HFD-induced macrophage infiltration and inflammatory cytokine expression in adipose tissue. **(a)** Representative findings of immunohistochemical staining for infiltrated macrophages by F4/80 antibody (black arrows) in epididymal fat; scale bar, 100 μ m. **(b)** Semi-quantitative analysis of the F4/80-positive cells. Values are expressed as mean \pm SD; ** p < 0.01; n = 8 in each group. **(c–e)** Quantification of *F4/80* **(c)**, *Cd68* **(d)** and *Cd11c* **(e)** mRNA in the fat of mice in each group. Values are expressed as mean \pm SD; * p < 0.05, ** p < 0.01; n = 12 in each group. **(f–k)** Quantitative analysis of mRNA expression for inflammatory cytokines *Tnf- α* **(f)**, *Mcp-1* **(g)**, *Il-1 β* **(h)**, *Il-6* **(i)**, and adipokines adiponectin **(j)** and leptin **(k)**, in the fat of mice in each group. Values are expressed as mean \pm SD; * p < 0.05, ** p < 0.01; n = 12 in each group **(l,m)** Plasma concentration of TNF- α **(l)** and adiponectin **(m)**. Values are expressed as mean \pm SD; * p < 0.05, ** p < 0.01; n = 12 in each group



LysM-Cre *Fth* KO mice (Fig. 8a–e). LPS stimulation increased *Tnf- α* mRNA expression, and it was partly inhibited with *Fth* siRNA transduction (Fig. 8f).

Discussion

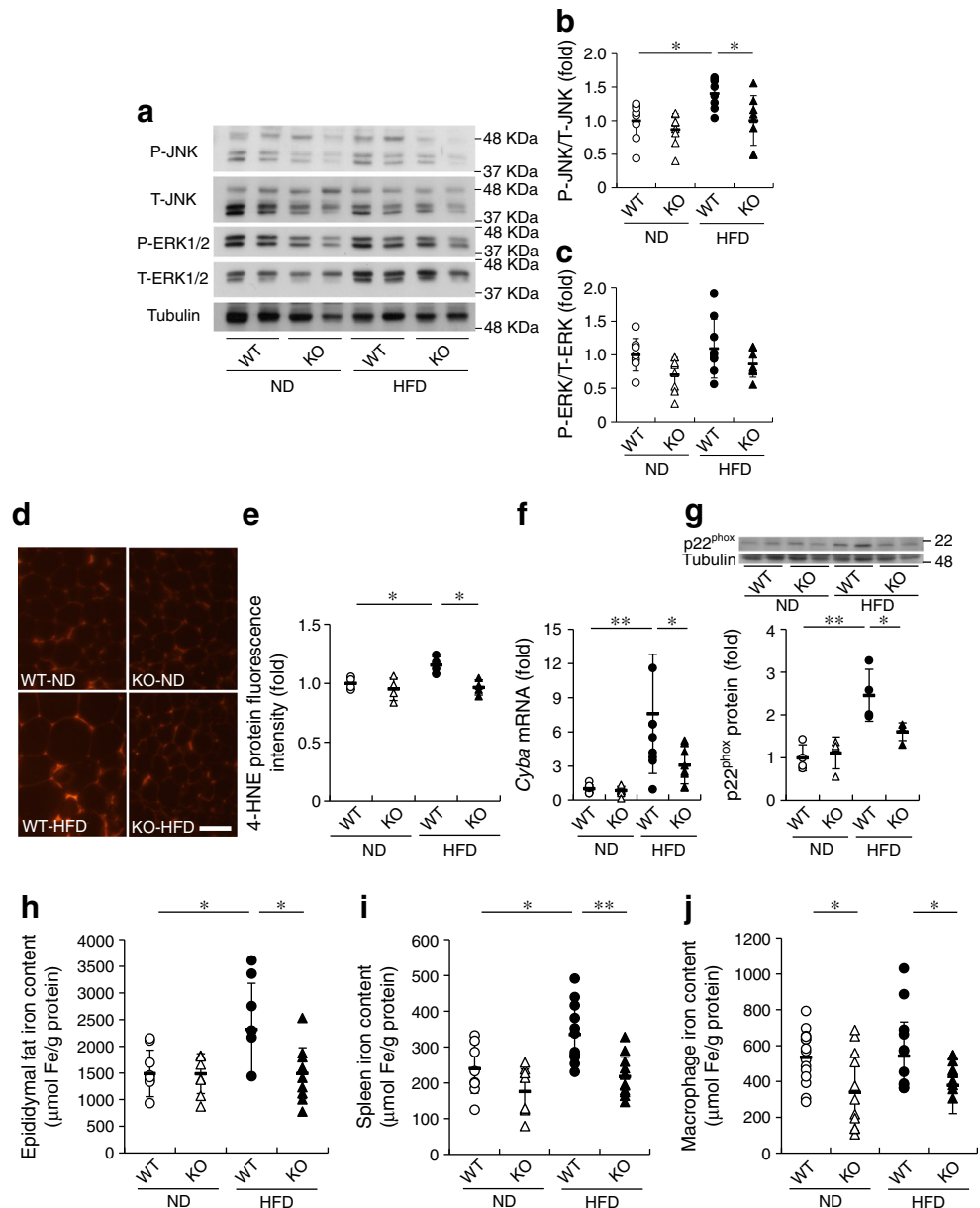
Deletion of the macrophage *Fth* gene reduced intracellular iron content via changes in iron transporter expression and inhibited the LPS-induced inflammatory response. Macrophage *Fth* gene KO mice showed diminished HFD-induced inflammatory changes and macrophage infiltration

in adipose tissue, contributing to the suppression of obesity and diabetes.

Ferritin is a ubiquitous iron-binding protein and the main form of intracellular iron storage. It is composed of 24-mer heteromultimers of two subtypes: H (FTH) and L (FTL) subunits [24]. FTH has ferroxidase activity (converts Fe²⁺ to Fe³⁺). Meanwhile, FTL takes up and maintains iron content by nucleation, although it lacks ferroxidase activity [25–27]. Ferritin synthase is mainly regulated by iron at the translational level through both iron-regulatory proteins and iron-responsive elements in the 5'-untranslated regions of *Fth* and *Ftl* RNAs [28], and in an iron-independent manner including

Fig. 4 Effect of macrophage *Fth* deletion on JNK and ERK signalling pathway.

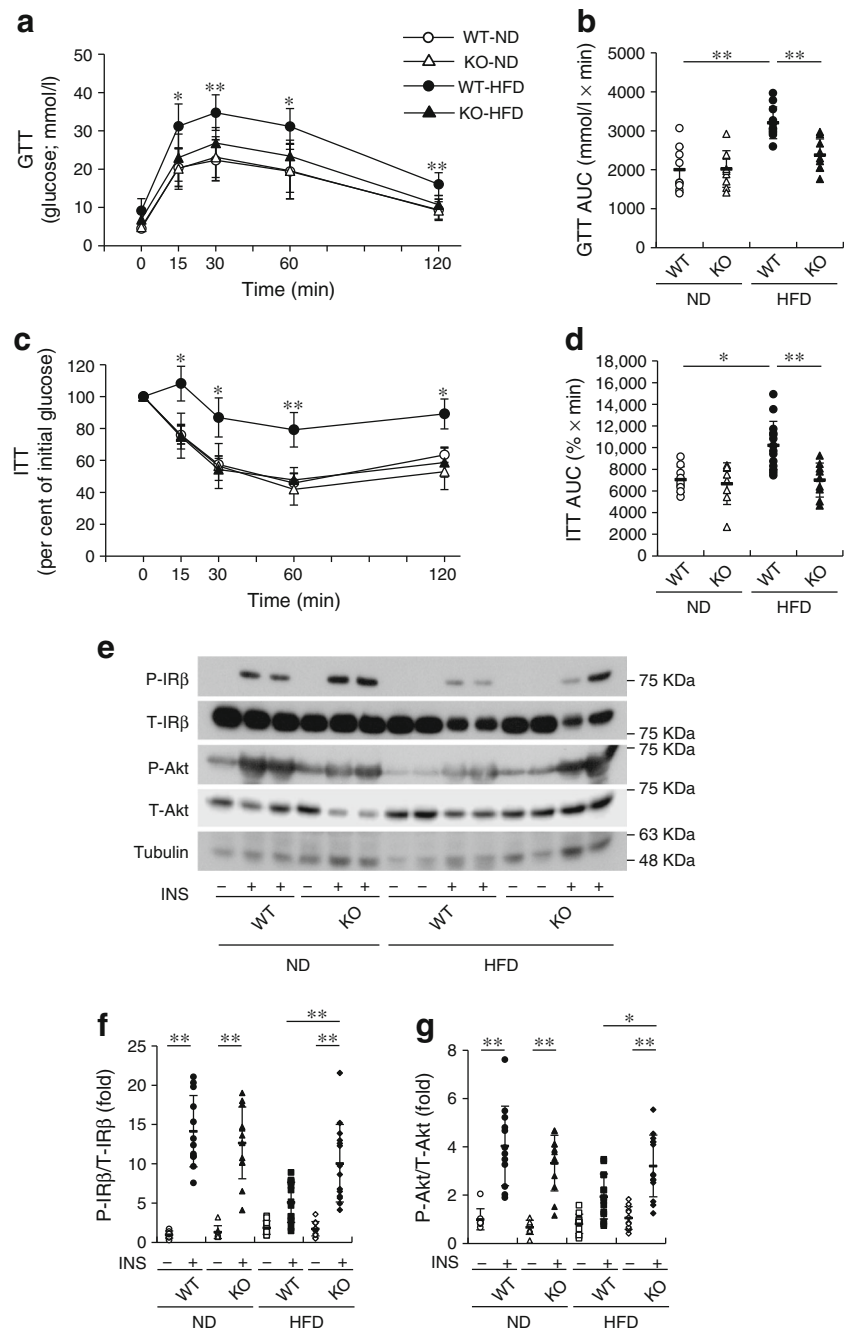
(a) Representative protein bands of phosphorylated JNK, total (T) JNK, phosphorylated ERK1/2, total ERK1/2 and tubulin in epididymal fat of each mouse group. (b, c) Semi-quantitative analysis of densitometry for JNK (b) and ERK1/2 (c) phosphorylation. Values are expressed as mean \pm SD. * p < 0.05; n = 8 in each group. (d, e) Lipid peroxidation in epididymal adipose tissue. (d) Representative findings of immunohistochemistry for 4-HNE; scale bar, 100 μ m. (e) Semi-quantitative analysis of 4-HNE-positive intensity. Values are expressed as mean \pm SD. * p < 0.05; n = 4. (f, g) NADPH oxidase expression in epididymal adipose tissue. mRNA and protein expression of p22^{phox} in epididymal fat. (f) quantitative analysis of *Cyba* mRNA (encoding p22^{phox}) expression. Values are expressed as mean \pm SD; * p < 0.05, ** p < 0.01; n = 8. (g) Representative images and semi-quantitative analysis of p22^{phox} protein expression. Values are expressed as mean \pm SD; * p < 0.05, ** p < 0.01; n = 4. (h–j) Measurement of iron content in epididymal fat (h), spleen (i) and peritoneal macrophages (j) of each mouse group. Values are expressed as mean \pm SD; * p < 0.05, ** p < 0.01; n = 8–20 in each group



oxidative stress [29], and in the presence of inflammatory cytokines [30, 31]. In addition to being an iron-storage protein, FTH is normally thought to exert a cytoprotective effect by its antioxidant property, inhibiting the Fenton reaction via ferroxidase activity and the nucleation of free iron ions [26, 27]. Indeed, several studies have shown the protective action of FTH in relation to heart failure (in cardiomyocytes) [32], acute kidney injury (proximal tubules) [33], and ischaemic liver injury (hepatocytes) [34]. In contrast, myeloid (macrophage) *Fth* gene deficiency alleviates unilateral ureter obstruction-induced renal fibrosis in mice, although the mechanism has not been described in detail [35]. Thus, FTH function might vary depending on cells and tissues, and macrophage *Fth* deletion exerts a favourable effect on at least renal fibrosis, obesity and diabetes.

Whole-body iron reduction by an iron chelator or an iron-restricted diet has been shown to be beneficial for the inhibition of inflammatory cytokines and oxidative stress in rat and mouse models of obesity and type 2 diabetes [11, 36, 37]. However, these advantages are counterbalanced by iron-deficient anaemia. In this study, macrophage deletion of the *Fth* gene resulted in reduced iron content, inhibiting the development of HFD-induced obesity and diabetes, inflammatory cytokines, macrophage infiltration and oxidative stress, without giving rise to anaemia. HFD-induced increase of proinflammatory cytokine expression (the M1-like markers: IL-1 β , TNF- α , CD68) was diminished in the fat of LysM-Cre *Fth* KO mice compared with WT mice. Similarly, LPS-induced increase of TNF- α expression was also alleviated in RAW264.7 macrophage cells transfected with *Fth* siRNA.

Fig. 5 Effect of macrophage *Fth* deletion on glucose tolerance and insulin sensitivity in mice. **(a)** Changes in blood glucose level during IPGTT in WT mice and LysM-Cre *Fth* KO mice fed with ND and HFD. Values are expressed as mean \pm SD; * p < 0.05, ** p < 0.01 for WT-HFD vs other groups; n = 8–11 in each group. **(b)** AUC of blood glucose level during IPGTT. Values are expressed as mean \pm SD; ** p < 0.01; n = 8–11 in each group. **(c)** Changes in blood glucose level during IPITT in WT mice and LysM-Cre *Fth* KO mice fed with ND and HFD. Values are expressed as mean \pm SD; * p < 0.05, ** p < 0.01 for WT-HFD vs other groups; n = 8–14 in each group. **(d)** AUC of blood glucose level during IPITT. Values are expressed as mean \pm SD; * p < 0.05, ** p < 0.01; n = 8–14 in each group. **(e–g)** Effect of macrophage *Fth* deletion on HFD-induced insulin resistance in epididymal fat. **(e)** Representative protein bands of phosphorylated IR β , total (T) IR β , phosphorylated Akt, total Akt and tubulin. Semi-quantitative analysis of densitometry for IR β **(f)** and Akt **(g)** phosphorylation in fat tissue. Values are expressed as mean \pm SD; * p < 0.05, ** p < 0.01; n = 8–14 in each group. INS, insulin

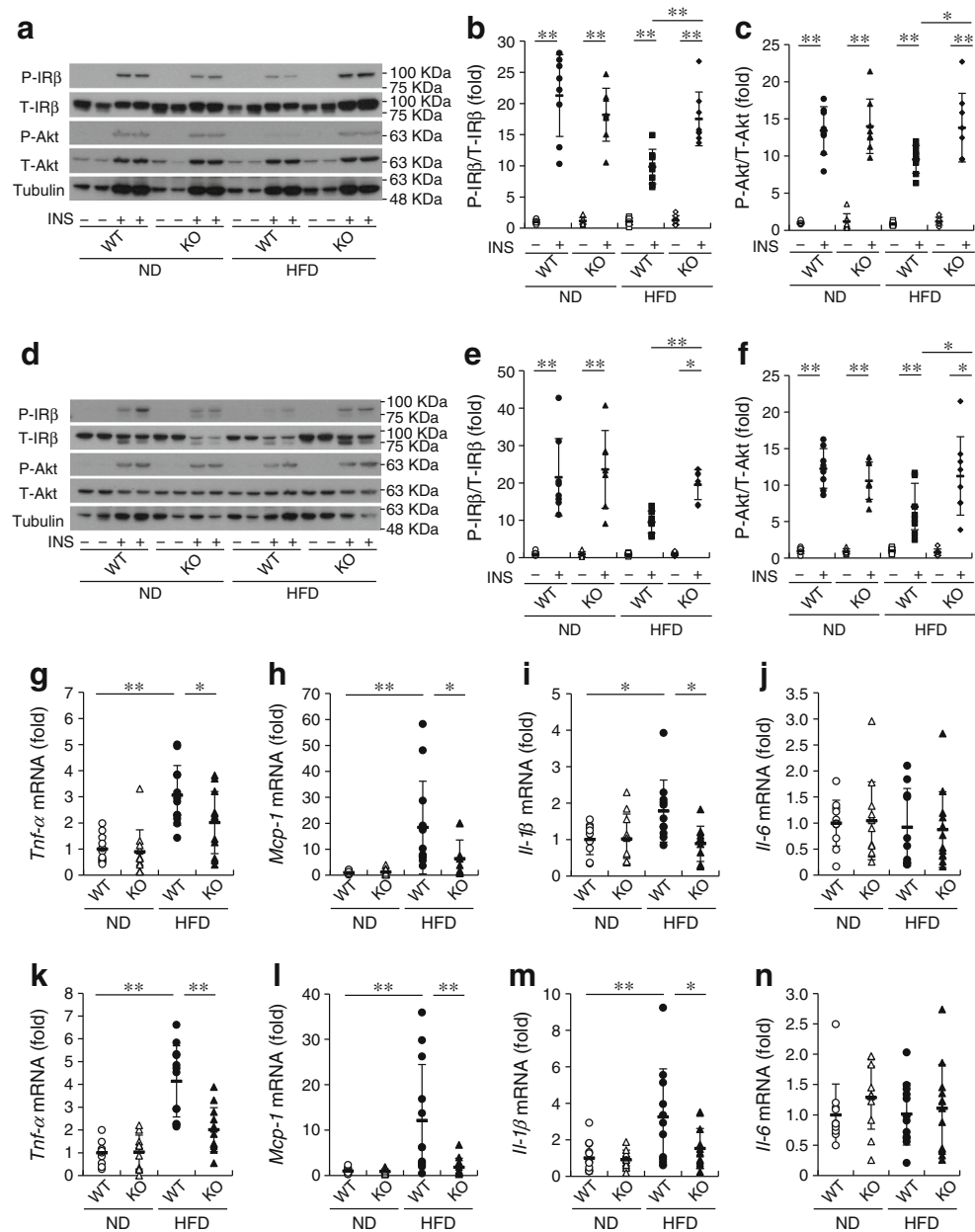


These findings suggest that macrophage iron plays a pivotal role in the development of obesity and diabetes, and macrophage-specific reduction of iron may be a target for metabolic disorders through the inhibition of the inflammatory response.

It is well established that chronic low-grade inflammation is linked to the development of insulin resistance, obesity and diabetes [38]. An increase of infiltrated macrophages is seen in the visceral fat of obese individuals, and body weight loss leads to a reduction of inflammatory markers and infiltrated macrophages [39, 40]. Diet-induced obesity promotes

macrophages to switch to the M1 proinflammatory phenotype from the M2 anti-inflammatory phenotype, contributing to insulin resistance [41]. A shift in the polarisation of adipose tissue macrophages to a proinflammatory phenotype plays a crucial role in the development of obesity and diabetes. Deletion of the *Fth* gene altered the expression of iron-related genes (decrease of *Tfr* expression and the increase of *Fpn* and *Homx1* expression) in addition to iron content reduction. Iron metabolism is suggested to involve the regulation of macrophage polarisation. M1-polarised proinflammatory macrophages increase intracellular iron retention with

Fig. 6 Effect of macrophage *Fth* deletion on insulin sensitivity and inflammatory cytokines in liver and skeletal muscle of mice. **(a)** Representative protein bands of phosphorylated IR β , total (T) IR β , phosphorylated Akt, total Akt and tubulin in the liver. **(b, c)** Semi-quantitative analysis of densitometry for IR β **(b)** and Akt **(c)** phosphorylation in the liver. Values are expressed as mean \pm SD; * p <0.05, ** p <0.01; n = 8 in each group. **(d)** Representative protein bands of phosphorylated IR β , total IR β , phosphorylated Akt, total Akt and tubulin in skeletal muscle. **(e, f)** Semi-quantitative analysis of densitometry for IR β **(e)** and Akt **(f)** phosphorylation in skeletal muscle. Values are expressed as mean \pm SD; * p <0.05, ** p <0.01; n = 8 in each group. **(g–n)** Quantitative analysis of mRNA expression for inflammatory cytokines in the liver: *Tnf- α* **(g)**, *Mcp-1* **(h)**, *Il-1 β* **(i)**, *Il-6* **(j)**; and the skeletal muscle: *Tnf- α* **(k)**, *Mcp-1* **(l)**, *Il-1 β* **(m)**, *Il-6* **(n)**. Values are expressed as mean \pm SD; * p <0.05, ** p <0.01; n = 10–12 in each group. INS, insulin



reduction of transferrin receptor (TfR) and FPN and elevation of FTH, while, M2-polarised anti-inflammatory macrophages decrease intracellular iron content with elevation of TfR and FPN and reduction of FTH in vitro [18]. In vivo, in lean adipose tissue, all infiltrated macrophages with low or high iron content are of the M2-like phenotype with greater expression of M2 genes and a reduction in the expression of M1 genes, suggesting the promotion of iron recycling. In obesity, macrophages with high iron levels become more inflammatory and lose the property of iron handling, indicating changes in their polarisation and phenotype [42]. In this study, *Fth* gene deletion inhibited the proinflammatory response induced by HFD or LPS. However, the change of *TfR* expression was in contrast to the M2-like phenotype, and the increase of *Fpn*

and *Homx1* expression was agreement with it. However, the effect of FTH overexpression is controversial. FTH overexpression itself increases inducible nitric oxide synthase (iNOS) expression [35], while ferritin induction alleviates the LPS-induced inflammatory response [43]. Further investigation is necessary for clarifying the role of FTH on macrophages in detail.

We showed that *LysM-Cre Fth* KO mice had higher energy expenditure compared with WT mice following HFD feeding. The body temperature and expression of thermogenic genes in epididymal fat were also higher in HFD-fed KO mice compared with HFD-fed WT mice. White-to-brown fat transition (forming what are known as beige adipocytes) plays a significant role in regulating body weight and protecting

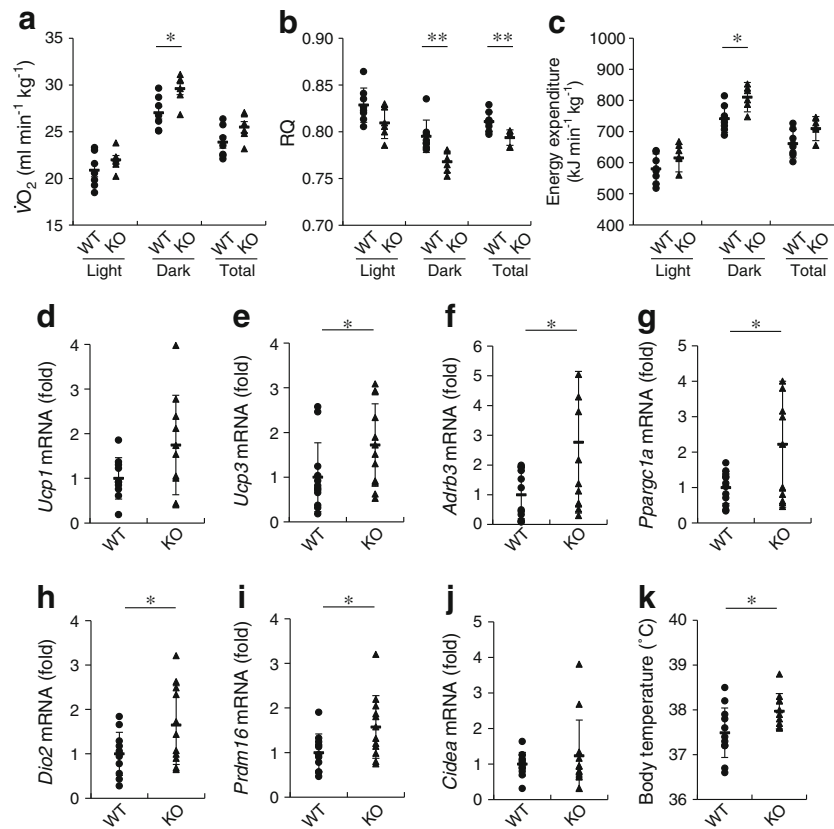
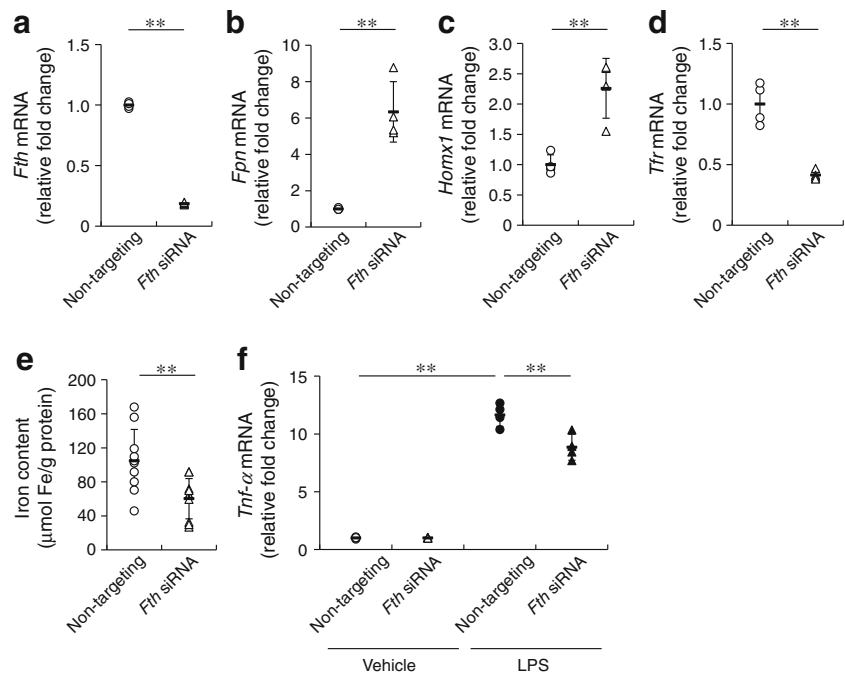


Fig. 7 Effect of macrophage *Fth* deletion on metabolic expenditure and thermogenesis in mice fed with HFD. (a) Effect of macrophage *Fth* deletion on $\dot{V}O_2$. Values are expressed as mean \pm SD. **p* < 0.05; *n* = 6–7 in each group. There was no significant difference in the total phase (light and dark) between WT and KO (*p* = 0.08). (b) Effect of macrophage *Fth* deletion on RQ. Values are expressed as mean \pm SD. ***p* < 0.01; *n* = 6–7 in each group. There was no significant difference in the light phase between WT and KO (*p* = 0.06). (c) Effect of macrophage *Fth* deletion

on energy expenditure. Values are expressed as mean \pm SD. **p* < 0.05; *n* = 6–7 in each group. There was no significant difference in the total phase between WT and KO (*p* = 0.1). (d–k) Effect of macrophage *Fth* deletion on thermogenic gene expression and body temperature in mice fed with HFD. (d–j) Thermogenic gene expression in epididymal fat of mice fed with HFD. Values are expressed as mean \pm SD. **p* < 0.05; *n* = 10–12 in each group. (k) Body temperature in mice following HFD feeding. Values are expressed as mean \pm SD; **p* < 0.05; *n* = 12 in each group

Fig. 8 Effect of RNA interference to *Fth* gene on LPS-induced inflammatory cytokine expression in RAW264.7 cells. (a–d) mRNA expression of *Fth* (a), *Fpn* (b), *Homx1* (c) and *Tfr* (d) in macrophages transfected with non-targeting siRNA or *Fth* siRNA. Values are expressed as mean \pm SD. ***p* < 0.01; *n* = 4 in each group (e) Iron content following control siRNA or *Fth* siRNA transfection. Values are expressed as mean \pm SD; ***p* < 0.01; *n* = 10 in each group. (f) LPS-induced *Tnf- α* mRNA expression in macrophages with unrelated control siRNA or *Fth* siRNA transfection. Values are expressed as mean \pm SD. ***p* < 0.01; *n* = 4 in each group



against diabetes and obesity through thermogenesis [44]. Therefore, the promotion of browning of white fat may partly involve the alleviation of HFD-induced obesity and diabetes in *LysM-Cre Fth* KO mice.

In terms of tissue iron content, the HFD induced an increase of tissue iron concentration in epididymal fat and spleen of WT mice, but the increase in iron concentration induced by HFD was suppressed in *LysM-Cre Fth* KO mice. However, iron content was not increased by HFD in isolated peritoneal macrophages, although macrophage iron content remained lower in KO mice than in WT mice with either ND or HFD. Increased iron content in fat and spleen might be due to the increase in infiltrated macrophages that supply iron to local tissues in mice following HFD. In *in vitro* models, M1 macrophages display an iron sequestration phenotype with an associated increase in FTH expression. Similar results were obtained in mouse models where the iron content of macrophages of both subtypes was not increased by HFD administration, although the iron content was increased in HFD-induced hypertrophied adipocytes [42]. Thus, there is the discrepancy of M1 macrophage iron content between the *in vitro* model and *in vivo* model. In contrast, macrophage iron release is necessary for the repair of skeletal muscle injury through myogenic differentiation. There are no differences in macrophage iron content during muscle injury [45], suggesting that macrophages are the suppliers of iron to local tissue without themselves exhibiting any change in iron content, due to rapid iron release. Further studies are needed to clarify the accurate mechanism.

Body iron content is normally lower in females than males, and several studies have shown the effect of sex hormones on iron metabolism [22, 46]. A limitation of this study is that we only used male mice. Therefore, further study is necessary for clarifying the effect of *Fth* deletion on macrophages in both sexes.

In conclusion, deletion of the *Fth* gene in macrophages leads to a reduction of both intracellular iron concentration and inflammatory response, resulting in the prevention of HFD-induced obesity and diabetes. Control of macrophage-specific iron levels is, thus, a potential therapeutic target for regulating chronic inflammation.

Acknowledgements We appreciate the excellent technical advice by the Support Centre for Advanced Medical Sciences, Institute of Biomedical Sciences, Tokushima University Graduate School. We would like to thank Editage (www.editage.jp) for their help with English language editing.

Data availability All data generated or analysed during this study are included in this published article.

Funding This work was supported by the Japan Society for the Promotion of Science (JSPS) KAKENHI Grant (18 K08480 to YI).

Authors' relationships and activities The authors declare that there are no relationships or activities that might bias, or be perceived to bias, their work.

Contribution statement YI conceived the study, designed experiments, acquired and analysed the data, and wrote the manuscript. HW, TS and HH acquired and analysed the data and drafted the manuscript. YH contributed to the analysis and interpretation of the data and reviewed the manuscript. MI, MG, YZ, KTa, YI-I, LM and KI contributed to the analysis and interpretation of the data and assisted in the preparation of the manuscript. K-iA and KTs contributed to analysis and interpretation of the data and critically reviewed the manuscript. TT contributed to interpretation of the data and critically reviewed the manuscript. YI and HW are the guarantors of this work and, as such, had full access to all the data in the study and take responsibility for the integrity of the data and the accuracy of the data analysis. All the authors approved the final version of this manuscript.

References

1. Camaschella C (2005) Understanding iron homeostasis through genetic analysis of hemochromatosis and related disorders. *Blood* 106(12):3710–3717. <https://doi.org/10.1182/blood-2005-05-1857>
2. Ryan Caballes F, Sendi H, Bonkovsky HL (2012) Hepatitis C, porphyria cutanea tarda and liver iron: an update. *Liver Int* 32(6):880–893. <https://doi.org/10.1111/j.1478-3231.2012.02794.x>
3. Dongiovanni P, Fracanzani AL, Fargion S, Valenti L (2011) Iron in fatty liver and in the metabolic syndrome: a promising therapeutic target. *J Hepatol* 55(4):920–932. <https://doi.org/10.1016/j.jhep.2011.05.008>
4. Nikonorov AA, Skalnaya MG, Tinkov AA, Skalny AV (2015) Mutual interaction between iron homeostasis and obesity pathogenesis. *J Trace Elem Med Biol* 30:207–214. <https://doi.org/10.1016/j.jtemb.2014.05.005>
5. Fernandez-Real JM, Manco M (2014) Effects of iron overload on chronic metabolic diseases. *Lancet Diabetes Endocrinol* 2(6):513–526. [https://doi.org/10.1016/S2213-8587\(13\)70174-8](https://doi.org/10.1016/S2213-8587(13)70174-8)
6. Kremastinos DT, Farmakis D (2011) Iron overload cardiomyopathy in clinical practice. *Circulation* 124(20):2253–2263. <https://doi.org/10.1161/CIRCULATIONAHA.111.050773>
7. Depalma RG, Hayes VW, Chow BK, Shamayeva G, May PE, Zacharski LR (2010) Ferritin levels, inflammatory biomarkers, and mortality in peripheral arterial disease: a substudy of the Iron (Fe) and Atherosclerosis Study (FeAST) Trial. *J Vasc Surg* 51(6):1498–1503. <https://doi.org/10.1016/j.jvs.2009.12.068>
8. Ribeiro S, Belo L, Reis F, Santos-Silva A (2016) Iron therapy in chronic kidney disease: recent changes, benefits and risks. *Blood Rev* 30(1):65–72. <https://doi.org/10.1016/j.blre.2015.07.006>
9. Nakanishi T, Kuragano T, Nanami M, Otaki Y, Nonoguchi H, Hasuike Y (2010) Importance of ferritin for optimizing anemia therapy in chronic kidney disease. *Am J Nephrol* 32(5):439–446. <https://doi.org/10.1159/000320733>
10. Beaton MD, Chakrabarti S, Levstik M, Speechley M, Marotta P, Adams P (2013) Phase II clinical trial of phlebotomy for non-alcoholic fatty liver disease. *Aliment Pharmacol Ther* 37(7):720–729. <https://doi.org/10.1111/apt.12255>
11. Tajima S, Ikeda Y, Sawada K et al (2012) Iron reduction by deferroxamine leads to amelioration of adiposity via the regulation of oxidative stress and inflammation in obese and type 2 diabetes KKAY mice. *Am J Physiol Endocrinol Metab* 302(1):E77–E86. <https://doi.org/10.1152/ajpendo.00033.2011>
12. Ikeda Y, Enomoto H, Tajima S et al (2013) Dietary iron restriction inhibits progression of diabetic nephropathy in *db/db* mice. *Am J Physiol Ren Physiol* 304(7):F1028–F1036. <https://doi.org/10.1152/ajprenal.00473.2012>
13. Ikeda Y, Horinouchi Y, Hamano H et al (2017) Dietary iron restriction alleviates renal tubulointerstitial injury induced by protein

- overload in mice. *Sci Rep* 7(1):10621. <https://doi.org/10.1038/s41598-017-11089-0>
14. Naito Y, Hirotsani S, Sawada H, Akahori H, Tsujino T, Masuyama T (2011) Dietary iron restriction prevents hypertensive cardiovascular remodeling in Dahl salt-sensitive rats. *Hypertension* 57(3):497–504. <https://doi.org/10.1161/HYPERTENSIONAHA.110.159681>
 15. Ganz T (2012) Macrophages and systemic iron homeostasis. *J Innate Immun* 4(5–6):446–453. <https://doi.org/10.1159/000336423>
 16. Mills CD, Kincaid K, Alt JM, Heilman MJ, Hill AM (2000) M-1/M-2 macrophages and the Th1/Th2 paradigm. *J Immunol* 164(12):6166–6173
 17. Recalcati S, Locati M, Marini A et al (2010) Differential regulation of iron homeostasis during human macrophage polarized activation. *Eur J Immunol* 40(3):824–835. <https://doi.org/10.1002/eji.200939889>
 18. Coma G, Campana L, Pignatti E et al (2010) Polarization dictates iron handling by inflammatory and alternatively activated macrophages. *Haematologica* 95(11):1814–1822. <https://doi.org/10.3324/haematol.2010.023879>
 19. Recalcati S, Locati M, Gammella E, Invernizzi P, Cairo G (2012) Iron levels in polarized macrophages: regulation of immunity and autoimmunity. *Autoimmun Rev* 11(12):883–889. <https://doi.org/10.1016/j.autrev.2012.03.003>
 20. Tsukamoto H, Lin M, Ohata M, Giulivi C, French SW, Brittenham G (1999) Iron primes hepatic macrophages for NF- κ B activation in alcoholic liver injury. *Am J Phys* 277(6):G1240–G1250. <https://doi.org/10.1152/ajpgi.1999.277.6.G1240>
 21. Autenrieth IB, Bohn E, Ewald JH, Heesemann J (1995) Deferoxamine B but not deferoxamine G1 inhibits cytokine production in murine bone marrow macrophages. *J Infect Dis* 172(2):490–496. <https://doi.org/10.1093/infdis/172.2.490>
 22. Ikeda Y, Tajima S, Izawa-Ishizawa Y et al (2012) Estrogen regulates hepcidin expression via GPR30-BMP6-dependent signaling in hepatocytes. *PLoS One* 7(7):e40465. <https://doi.org/10.1371/journal.pone.0040465>
 23. Li DQ, Luo L, Chen Z, Kim HS, Song XJ, Pflugfelder SC (2006) JNK and ERK MAP kinases mediate induction of IL-1 β , TNF- α and IL-8 following hyperosmolar stress in human limbal epithelial cells. *Exp Eye Res* 82(4):588–596. <https://doi.org/10.1016/j.exer.2005.08.019>
 24. Harrison PM, Arosio P (1996) The ferritins: molecular properties, iron storage function and cellular regulation. *Biochim Biophys Acta* 1275(3):161–203. [https://doi.org/10.1016/0005-2728\(96\)00022-9](https://doi.org/10.1016/0005-2728(96)00022-9)
 25. Lawson DM, Artymiuk PJ, Yewdall SJ et al (1991) Solving the structure of human H ferritin by genetically engineering intermolecular crystal contacts. *Nature* 349(6309):541–544. <https://doi.org/10.1038/349541a0>
 26. Lawson DM, Treffry A, Artymiuk PJ et al (1989) Identification of the ferroxidase centre in ferritin. *FEBS Lett* 254(1–2):207–210. [https://doi.org/10.1016/0014-5793\(89\)81040-3](https://doi.org/10.1016/0014-5793(89)81040-3)
 27. Santambrogio P, Levi S, Cozzi A, Corsi B, Arosio P (1996) Evidence that the specificity of iron incorporation into homopolymers of human ferritin L- and H-chains is conferred by the nucleation and ferroxidase centres. *Biochem J* 314(Pt 1):139–144
 28. Klausner RD, Harford JB (1989) *cis-trans* models for post-transcriptional gene regulation. *Science* 246(4932):870–872. <https://doi.org/10.1126/science.2683086>
 29. Tsuji Y, Ayaki H, Whitman SP, Morrow CS, Torti SV, Torti FM (2000) Coordinate transcriptional and translational regulation of ferritin in response to oxidative stress. *Mol Cell Biol* 20(16):5818–5827. <https://doi.org/10.1128/mcb.20.16.5818-5827.2000>
 30. Miller LL, Miller SC, Torti SV, Tsuji Y, Torti FM (1991) Iron-independent induction of ferritin H chain by tumor necrosis factor. *Proc Natl Acad Sci U S A* 88(11):4946–4950. <https://doi.org/10.1073/pnas.88.11.4946>
 31. Rogers JT (1996) Ferritin translation by interleukin-1 and interleukin-6: the role of sequences upstream of the start codons of the heavy and light subunit genes. *Blood* 87(6):2525–2537
 32. Omiya S, Hikoso S, Imanishi Y et al (2009) Downregulation of ferritin heavy chain increases labile iron pool, oxidative stress and cell death in cardiomyocytes. *J Mol Cell Cardiol* 46(1):59–66. <https://doi.org/10.1016/j.yjmcc.2008.09.714>
 33. Zarjou A, Bolisetty S, Joseph R et al (2013) Proximal tubule H-ferritin mediates iron trafficking in acute kidney injury. *J Clin Invest* 123(10):4423–4434. <https://doi.org/10.1172/JCI67867>
 34. Berberat PO, Katori M, Kaczmarek E et al (2003) Heavy chain ferritin acts as an antiapoptotic gene that protects livers from ischemia reperfusion injury. *FASEB J* 17(12):1724–1726. <https://doi.org/10.1096/fj.03-0229fje>
 35. Bolisetty S, Zarjou A, Hull TD et al (2015) Macrophage and epithelial cell H-ferritin expression regulates renal inflammation. *Kidney Int* 88(1):95–108. <https://doi.org/10.1038/ki.2015.102>
 36. Minamiyama Y, Takemura S, Kodai S et al (2010) Iron restriction improves type 2 diabetes mellitus in Otsuka Long-Evans Tokushima fatty rats. *Am J Physiol Endocrinol Metab* 298(6):E1140–E1149. <https://doi.org/10.1152/ajpendo.00620.2009>
 37. Yan HF, Liu ZY, Guan ZA, Guo C (2018) Deferoxamine ameliorates adipocyte dysfunction by modulating iron metabolism in *ob/ob* mice. *Endocr Connect* 7(4):604–616. <https://doi.org/10.1530/EC-18-0054>
 38. Dandona P, Aljada A, Bandyopadhyay A (2004) Inflammation: the link between insulin resistance, obesity and diabetes. *Trends Immunol* 25(1):4–7. <https://doi.org/10.1016/j.it.2003.10.013>
 39. Canello R, Henegar C, Viguier N et al (2005) Reduction of macrophage infiltration and chemoattractant gene expression changes in white adipose tissue of morbidly obese subjects after surgery-induced weight loss. *Diabetes* 54(8):2277–2286. <https://doi.org/10.2337/diabetes.54.8.2277>
 40. Canello R, Tordjman J, Poitou C et al (2006) Increased infiltration of macrophages in omental adipose tissue is associated with marked hepatic lesions in morbid human obesity. *Diabetes* 55(6):1554–1561. <https://doi.org/10.2337/db06-0133>
 41. Lumeng CN, Bodzin JL, Saltiel AR (2007) Obesity induces a phenotypic switch in adipose tissue macrophage polarization. *J Clin Invest* 117(1):175–184. <https://doi.org/10.1172/JCI29881>
 42. Orr JS, Kennedy A, Anderson-Baucum EK et al (2014) Obesity alters adipose tissue macrophage iron content and tissue iron distribution. *Diabetes* 63(2):421–432. <https://doi.org/10.2337/db13-0213>
 43. Zarjou A, Black LM, McCullough KR et al (2019) Ferritin light chain confers protection against sepsis-induced inflammation and organ injury. *Front Immunol* 10:131. <https://doi.org/10.3389/fimmu.2019.00131>
 44. Wu J, Bostrom P, Sparks LM et al (2012) Beige adipocytes are a distinct type of thermogenic fat cell in mouse and human. *Cell* 150(2):366–376. <https://doi.org/10.1016/j.cell.2012.05.016>
 45. Coma G, Caserta I, Monno A et al (2016) The repair of skeletal muscle requires iron recycling through macrophage ferroportin. *J Immunol* 197(5):1914–1925. <https://doi.org/10.4049/jimmunol.1501417>
 46. Guo W, Bachman E, Li M et al (2013) Testosterone administration inhibits hepcidin transcription and is associated with increased iron incorporation into red blood cells. *Aging Cell* 12(2):280–291. <https://doi.org/10.1111/acel.12052>

Publisher's note Springer Nature remains neutral with regard to jurisdictional claims in published maps and institutional affiliations.